EUROPEAN ORGANIZATION FOR NUCLEAR RESEARCH

May 20, 2017

D-hadron correlations in p-Pb collisions at $\sqrt{s_{\rm NN}}$ = 5.02 TeV

F. Colamaria, S. Kumar, M. Mazzilli

Abstract

In this note, we present the analysis of azimuthal correlations of D mesons and primary charged particles performed in the ALICE central barrel in p-Pb collisions at $\sqrt{s_{NN}}$ = 5.02 TeV, from 2016 data taking, in an extended $p_{\rm T}$ range and with additional observables with respect to p-Pb 2013 data analysis. After a description of the analysis strategy, corrections and systematic uncertainties, the results obtained for prompt $\rm D^0$, $\rm D^{*+}$ and $\rm D^+$mesons in different ranges of transverse momentum of the D meson and of the associated particles are presented and compared to Monte Carlo models and, for the common $p_{\rm T}$ ranges and observables, to 2013 p-Pb analysis.

Contents

1 Introduction and Motivation

The study of the azimuthal correlations of heavy-flavoured particles and charged particles at the LHC energies provides a way to characterize charm production and fragmentation processes in pp collisions as well as a way to probe our understanding of QCD in the perturbative regime, accessible in a large kinematic range given the large mass of heavy quarks. Flavour conservation in QCD implies that charm quarks are always produced as pairs of quarks and anti-quarks. The azimuthal correlations obtained using a meson carrying a heavy quark as trigger particle with the other charged particles in the same event give the possibility to study the underlying charm production mechanism in detail. In particular, prompt charm quark-antiquark pair production leads back to back in azimuth at first order in leading-order perturbative-QCD (pQCD). Heavy quarks produced from the splitting of a massless gluon can be rather collimated and may generate sprays of hadrons at small $\Delta\phi$. Finally, for hard-scattering topologies classified as "flavour-excitation", a charm quark undergoes a hard interaction from an initial splitting ($g \rightarrow c\bar{c}$), leading to a big separation in rapidity of the hadrons originating from the antiquark (quark) with respect to the trigger D meson and contribute to a rather flat term to the $\Delta\phi$-correlation distribution.

Heavy-flavour correlation studies in more complex collisional systems, like Pb-Pb, play a crucial role in studying the modification of the fragmentation of charmed jets due to in-medium (or cold nuclear matter, in case of p-Pb collisions) effects, in a similar way as it was done for di-hadron correlation studies in heavy-ion collisions (see for example [4, 5]). Furthermore, the recent observation of long range correlations in p-Pb for light flavour hadrons and for heavy-flavour decay electrons [1] points to possible collective effects or effects originating from gluon saturation in the initial state. More information could be extracted by the eventual observation of the same effect with D mesons.

In the following, we describe the analysis strategy for p-Pb in all its steps, and we describe the list of corrections and the estimation of the systematic uncertainties done. We then present the results of $\Delta\phi$ correlations, and quantitative observable extracted to fits to those distributions, obtained for prompt D^0, D^+ and D^{*+} in different ranges of transverse momentum for the D-meson (trigger particle) and the associated particles.

2 Data/Monte Carlo samples and event selection

The data samples used for the analyses were the FAST and CENT_woSDD samples from periods LHC16q and LHC16t (merged AOD samples). The reason for this choice is explained later on. It was verified, by looking at D-meson and track η and ϕ distributions, and at the mixed-event correlation distributions for each subsamples, that no visible differences arose for the four periods, hence it was possible to perform the analysis directly on the merged samples without any bias.

The Monte Carlo productions adopted for this study were:

1. LHC17d2a_fast_new, a HIJING production with enrichment, for each event, of c OR b quarks and their decay chains, performed by PYTHIA6 with Perugia2011 tune, and with forced hadronic decays of the charmed hadrons. This production was used for D-meson efficiency evaluation, purity estimation and Monte Carlo closure test.

2. LHC17a2b_cent_woSDD and LHC17a2b_fast, minimum-bias productions perfomed with DPMJET generator, used for the evaluation of the tracking efficiency.

Table 1 shows the list of runs used for the analysis, for each of the data taking periods, and of the Monte Carlo productions used to evaluate the corrections:

The trigger mask request for the event selection is kINT7. Only events with a reconstructed primary vertex within 10 cm from the centre of the detector along the beam line are considered for both pp and pPb collisions. This choice maximises the detector coverage of the selected events, considering the longitudinal size of the interaction region, and the detector pseudorapidity acceptances. For pPb collisions, the center-of-mass reference frame of the nucleon-nucleon collision is shifted in rapidity by $y_{\rm NN}$ = 0.465 in the proton direction with respect to the laboratory frame, due to the different per-nucleon energies of the proton and the lead beams. Beam-gas events are removed by offline selections based on the timing information provided by the V0 and the Zero Degree Calorimeters, and the correlation between the number of hits and track segments in the SPD detector. This is automatically performed in the Physic Selection, a positive outcome of which is required during our event selection. The minimum-bias trigger efficiency is 100% for events with D mesons with $p_{\rm T} > 1$ GeV/c. For the analyzed data samples, the probability of pile-up from collisions in the same bunch crossing is below 2% per triggered event (in most of the runs, well below 1%). Events in which more than one primary interaction vertex is reconstructed with the SPD detector (with minimum of 5 contributors, and a z distance greater than 0.8 cm) are rejected, which effectively removes the impact of in-bunch pile-up events on the analysis. Out-of-bunch tracks are effectively rejected by the request of at least one point in the SPD, which has a very limited time acquisition window (300 ns). Indeed, though the default associated track selection requires a minimum of 2 points in the ITS, as it will be shown later on full compatibility of the corrected results with 2 and 3 minimum ITS clusters is obtained. For FAST and CENT_woSDD samples, the latter case indirectly forces the presence of a point in the SPD.

A SMALL DISCUSSION FOR wsdd VS wosdd SAMPLES MUST BE DONE, WITH THE REASONING OF OUR FINAL CHOICE (WITH PLOTS FOR AT LEAST ONE MESON, BUT BETTER BOTH D+ and D*). YOU CAN PICK THE PLOTS FROM SHYAM AND MARIANNA'S TALKS!!

Type	Production	Run list	nEvents
Monte-Carlo	LHC17d2a_fast_new/AOD (c/b enriched), LHC17a2b_fast (MB), LHC17a2b_cent_woSDD (MB)	265525, 265521, 265501, 265500, 265499, 265435, 265427, 265426, 265425, 265424, 265422, 265421, 265420, 265419, 265388, 265387, 265385, 265384, 265383, 265381, 265378, 265377, 265344, 265343, 265342, 265339, 265338, 265336, 265335, 265334, 265332, 265309, 267165, 267164, 267163, 267166 = **[22 runs]**	??M
Data	"LHC16q, pass1_CENT_woSDD/AOD"	265525, 265521, 265501, 265500, 265499, 265435, 265427, 265426, 265425, 265424, 265422, 265421, 265420, 265419, 265388, 265387, 265385, 265384, 265383, 265381, 265378, 265377, 265344, 265343, 265342, 265339, 265338, 265336, 265335, 265334, 265332, 265309 = **[32 runs]**	261M total
	"LHC16q, pass1_FAST/AOD"	265525, 265521, 265501, 265500, 265499, 265435, 265427, 265426, 265425, 265424, 265422, 265421, 265420, 265419, 265388, 265387, 265385, 265384, 265383, 265381, 265378, 265377, 265344, 265343, 265342, 265339, 265338, 265336, 265335, 265334, 265332, 265309 = **[32 runs]**	260M
	"LHC16t, pass1_CENT_woSDD/AOD"	267166, 267165, 267164, 267163 = **[4 runs]**	40M
	"LHC16t, pass1_FAST/AOD"	267166, 267165, 267164, 267163 = **[4 runs]**	41M

Table 1: Data Set and Run list

3 Analysis strategy

The analysis strategy follows the one used from 2013 p-Pb data sample. Correlation pairs are formed by trigger particles (D mesons) reconstructed and selected in the following $p_{\mathrm{T}}^{\mathrm{trig}}$ ranges: $3 < p_{\mathrm{T}}^{\mathrm{trig}} < 5$, $5 < p_{\mathrm{T}}^{\mathrm{trig}} < 8$, $8 < p_{\mathrm{T}}^{\mathrm{trig}} < 16$, $16 < p_{\mathrm{T}}^{\mathrm{trig}} < 24$ GeV/c, and associated particles (charged tracks) for the following $p_{\mathrm{T}}^{\mathrm{assoc}}$ regions: $p_{\mathrm{T}}^{\mathrm{assoc}} > 0.3$, $0.3 < p_{\mathrm{T}}^{\mathrm{assoc}} < 1$, $1 < p_{\mathrm{T}}^{\mathrm{assoc}} < 2$, $2 < p_{\mathrm{T}}^{\mathrm{assoc}} < 3$, $p_{\mathrm{T}}^{\mathrm{assoc}} > 3$ GeV/c (with the addition of $p_{\mathrm{T}}^{\mathrm{assoc}} > 1$ GeV/c for comparison with p-Pb 2013 results). In D meson correlations, the particle identification defines the trigger particle rather than a momentum cut and therefore the momentum range of the associated particles is not constrained by that of the trigger particle. Our definition of associated particle includes any charged particle coming from the primary vertex of interaction, including those coming from strong and electromagnetic decay of unstable particles, and particles deriving from the decay of hadrons with charm or beauty. We therefore include any charged particle except those coming from weak decays of strange particles and particles produced in the interaction with the detector material. This definition corresponds to that used in the method AliAODMCParticle::IsPyhysicalPrimary(). All associated particles surviving the selection cuts and not matching the adopted criterion are considered as a contamination whose contribution has to be corrected for.

The analysis is performed through the following steps:

1. **D meson selection and signal extraction.** For each single event, "trigger" particles are defined as the selected D meson candidates (D^0, D^+ and D^{*+}) within a given p_T^{trig} range. The detection strategy for D mesons at central rapidity is the same as that described in [6] and is based on the reconstruction of decay vertices displayed from the primary vertex by a few hundred μm and on the identification of the decay-particle species. The identification of the charged kaon and pion in the TPC and TOF detectors helps to further reduce the background at low p_T. An invariant-mass analysis is then used to extract the raw signal yield, using the same fit functions described in [6].

   The D mesons are selected in the rapidity range varying from $|y| < 0.5$ at low p_T to $|y| < 0.8$ for $p_T > 5$ GeV/c.

2. **Correlation of D candidates with associated tracks.** Particle pairs are formed by associating each trigger particle with the charged primary particles passing the track selection (excluding those coming from the decay of the D-meson candidate) in a specified p_T^{assoc} interval (which can overlap with the p_T^{trig} range) and in the pseudo-rapidity range $|\eta| < 0.8$. For the D^0 meson, also the low-momnetum pion tracks from feed-down of D^{*+} mesons are removed via 3σ invariant mass cut on the $M(K\pi\pi) - M(K\pi)$ difference. This because these soft pion are not related to the charm quark fragmentation chain. For D meson candidates in the invariant mass signal region, defined by a $\pm$ 2σ interval around the D meson mass, the azimuthal angle difference $\phi^{assoc} - \phi^{trigg} \equiv \Delta\phi$ and the pseudorapidity difference $\eta^{assoc} - \eta^{trig} \equiv \Delta\eta$ are evaluated and stored to build two-dimensional correlation distribution.

   ADD: CUT OPTIMIZATION PARAGRAPH FOR D0, WITH SOME PLOT- PUT A REFERENCE TO MY LAST CUT OPT TALK, ON 22 MARCH HFCJ; CUT MODIFICATIONS (JUST AS TEXT, OR WITH 1-2 PLOTS) FOR D+; SAY THAT D+ HAS STD D"H p-Pb 2013 CUTS INSTEAD

3. **Correction for limited acceptance and detector inhomogeneities with Event Mixing** The angular correlation distribution may be affected, even for uncorrelated pair of particles, by structures not due to physical effects, but originating from the limited detector acceptance, as well as from angular inhomogeneities in the trigger and track reconstruction efficiencies as a function of $\Delta\phi$ and $\Delta\eta$. Effects of this kind are removed using the Event Mixing technique. In details, the analysis is executed on the same data sample of the standard one (called "same event" analysis, SE), but the trigger particles found in each event are correlated to charged particles reconstructed in different events ("Mixed Events" analysis, ME) with similar characteristic, in particular concerning the event multiplicity and z position of the primary vertex (see Section 3.2.1.

   The differential yield of associated particles per trigger particle is obtained by

$$\frac{1}{N_{\rm trig}} \frac{{\rm d}^2 N^{\rm pair}}{{\rm d}\Delta\eta\, {\rm d}\Delta\phi} = B_{ME}(0,0) \times \frac{S(\Delta\eta,\Delta\phi)}{B_{ME}(\Delta\eta,\Delta\phi)}, \tag{1}$$

   where $N^{\rm pair}$ is the total number of correlated D-hadron pairs. The functions $S(\Delta\eta,\Delta\phi)$ and $B_{ME}(\Delta\eta,\Delta\phi)$ are the signal and the mixed event background distributions, respectively. The latter is normalized to its value in $(\Delta\eta,\Delta\phi) = (0,0)$, i.e. $(B(0,0))$. Further details on the mixed-event correction are provided further on.

   The signal distribution is the per-trigger-particle yield of pairs found in the same event,

$$S(\Delta\eta,\Delta\phi) = \frac{1}{N_{\rm trig}} \frac{{\rm d}^2 N^{\rm same}}{{\rm d}\Delta\eta\, {\rm d}\Delta\phi}, \tag{2}$$

   where $N^{\rm same}$ is the number of such pairs within a ($\Delta\eta$,$\Delta\phi$) bin, divided by the product of the $\Delta\eta$ and $\Delta\phi$ bin widths.

The background distribution from mixed-event is given by

$$B_{ME}(\Delta\eta,\Delta\phi) = \frac{1}{N_{\rm trig}} \frac{{\rm d}^2 N^{\rm mix}}{{\rm d}\Delta\eta\,{\rm d}\Delta\phi}, \quad (3)$$

where $N^{\rm mix}$ denotes the number of mixed-event pairs. The ratio $B(0,0)/B(\Delta\eta,\Delta\phi)$ determines the pair acceptance correction factor. Multiplying the signal distribution by this ratio gives the acceptance-corrected per-trigger-particle associated yield.

4. **Subtraction of background correlation from signal distribution.** The invariant mass signal region includes also background D-meson candidates. Their contribution to the raw correlation distribution is subtracted as follows. For each $p_{\rm T}$ bin, the mean and the sigma of the invariant mass spectrum are extracted. For $\rm D^0$ and $\rm D^+$, a "background" region is defined in the sidebands of the mass distribution as the interval $4{\rm GeV}/c^2 < |m - m^{\rm pdg}| < 8{\rm GeV}/c^2$ (for the $\rm D^{*+}$ meson, only the right sideband is used). The angular correlation distribution for background candidates in this region is extracted and normalized with respect to the background in the signal region estimated from the mass fit. This normalized background correlation distribution is then subtracted from the raw signal one to obtain the signal correlation distribution. The normalization factor is the ratio of the number of background candidates under the signal peak (obtained bin-counting the candidates in the signal region and subtracting the integral of the fit function for the signal only, in the same range[1] **NOTE: THIS, AT LEAST FOR D0, SHALL BE REVERSED, SINCE WITH OPTIMIZED CUTS S >B IN MOST BINS. FOR D+ AND D*, PLEASE CHECK!!!**) over the number of background candidates in the sidebands (obtained via bin-counting in the sideband region). This normalized background correlation distribution is then subtracted from the raw signal one to obtain the signal correlation distribution.

   ADD PLOT OF 1D SIGNAL, SB, SIGNAL-SB REGION (I UPLOADED ONE EXAMPLE FOR D0)

5. **Correction for D meson efficiency and associated track efficiency.** After filling the signal and background correlation distributions, it is necessary to take into account also for the correlations with tracks not reconstructed, or not passing the quality selection due to poor reconstruction. In the same way, the loss of D-mesons which are not reconstructed, or do not pass the selection, impacts the correlation distribution shape. Hence, each pair is weighted by the inverse of the product of the associated track and D meson reconstruction efficiency, ε_{trk} and ε_{trig}. The associated track efficiency dependence on the particle pseudorapidity, transverse momentum, and z-coordinate of the primary vertex is taken into account. For the trigger particle efficiency only the $p_{\rm T}$ and the event multiplicity dependencies of the efficiency are considered, mainly to avoid large statistical fluctuations on the efficiency values arising when including also the dependency on η, due to the limited size of the Monte Carlo sample from which the D meson efficiencies are evaluated. The details of the efficiency corrections can be found in the following sections. To properly count the number of trigger particles used to normalize the correlation distributions, $N_{\rm trig}$, each D meson is weighted with the inverse of its efficiency in the invariant mass distribution. The main role of the correction for the D meson efficiency is to account for the $p_{\rm T}$ dependence of the correlation distribution within a given D meson $p_{\rm T}$ interval. Indeed, only the $p_{\rm T}$ shape of the D meson efficiency within the correlation $p_{\rm T}^{\rm trig}$ ranges is relevant while the average value in the $p_{\rm T}$ range is simplified due to the normalization of the correlation distribution to the number of trigger particles.

6. **Projection in $\Delta\phi$.** The limited statistics available does not allow to study the two dimensional $(\Delta\eta,\Delta\phi)$ distribution, which is therefore projected to the $\Delta\phi$ axis by integrating on $|\Delta\eta|$¡ 1. Despite, in principle, our maximum $\Delta\eta$ acceptance is of $|\Delta\eta|$¡ 1.6, removing the large $|\Delta\eta|$ regions

[1] With this procedure, the statistical fluctuations in the signal region are treated as background fluctuations. This is acceptable, since in most of the $p_{\rm T}$ ranges B > S, hence B fluctuations are higher than S fluctuations.

allow us to reject angular regions with very low statistics, where fluctuations would be amplified by a large mixed-event correction, and avoid the so-called wings effect.

As the difference in the azimuthal angle is periodic ($\Delta\phi = 0 = 2\pi$), the $\Delta\phi$-range is limited to the essential range of 2π. The $\Delta\phi$-limits are chosen to be $[-\pi/2,3\pi/2]$ in order to provide a good visibility of the correlation pattern, which peaks around 0 and π.

7. **Correction for the contamination of secondary particles** The DCA to primary vertex cut, applied during the associated track selection, has the role of removing the secondary particles from the associated track sample. Secondary particles are indeed produced either from long-lived strange hadrons or from interaction of particles with the detector material. A residual contamination from secondary tracks is hence expected in the correlation distributions. This contamination is estimated from Monte Carlo simulation based on Pythia as described more in detail in the next section. The background-subtracted event-mixing corrected correlations are multiplied by a purity factor to remove this contribution.

8. **Correction for feed-down of D meson from b-hadron decay** The selection strategy employed for the D meson candidates selection enhances the fraction of reconstructed D mesons coming from the decay of a b-hadron. Typical values, with the cuts used for the D-meson selection, are of the order of 10% or less. The correlation distribution of these secondary D mesons will be sensitive to the properties of beauty jets and beauty hadron decay, which in general differ from those relative to charm jets and hadrons. The procedure used to subtract this contribution is described in the next section.

9. **Study of correlation properties.** The properties of the azimuthal correlation distribution are quantified by fitting the distribution with a function composed of two Gaussian functions, modelling the near and the away side peaks, and a constant term describing the baseline. The mean of the Gaussian are fixed at $\Delta\phi = 0$ and $\Delta\phi = \pi$. To accomplish the 2π periodicity of the $\Delta\phi$ variable, the Gaussian functions are "duplicated" with mean at $\Delta\phi = 2\pi$ and $\Delta\phi = -\pi$. The fitting procedure is described in details the 5 section.

3.1 Code used for the analysis

The code used for D meson-hadron correlation analysis is fully committed in AliPhysics. The analysis classes can be found in \$ALICE_ROOT/PWGHF/correlationHF/. The D meson specific classes where the aforementioned steps are carried out are AliAnalysisTaskDStarCorrelations, AliAnalysisTaskSED0Correlations and AliAnalysisTaskDplusCorrelations. The classes which are common to the D meson specific analysis which includes the associated particle cuts and the correlation observables are AliHFAssociatedTrackCuts, AliHFCorrelator, AliHFOfflineCorrelator, AliReducedParticle and AliDhCorrelationExtraction. Several additional classes and macros in the same folder deal with the correction steps.

3.2 Corrections

3.2.1 Event Mixing

The event-mixing technique is used for correcting the raw correlation distribution for effects arising from the detector limited acceptance in rapidity and detector spatial inhomogeneities. The calculation of the Event Mixing correlation distribution is performed online. An event pool is created, where events preceding the one containing a D candidate are stored based on their properties (position of the vertex along the z axis and multiplicity). Each time a D meson candidate is found in an event, only the events contained in the same pool as the event under analysis is used to evaluate the correlations for the event mixing correction.

For D^0 and D^+, an offline approach for the mixed-event correction has been developed. In this approach, D-meson triggers and associated tracks from every analyzed event are stored in dedicated TTree, together with the needed kinematic information to build correlation distributions, and with identifiers of the events to which they belong. In this way, it is possible to correlate each D meson with all the tracks belonging to the same pool over the full event sample, and not being limited to the same subjob as for the online analysis. This allows to increase the statistics of the mixed-event correlation distributions. If was verified that online and offline approaches are fully compatible within the statistical uncertainties.

The multiplicity and z vertex position bins for the pools used in the p-Pb analysis (for both approaches) are the following:

- Multiplicity bins: $(0,40)\,;(40,65)\,;(65,+\infty)$
- Vertex z (cm) = $(-10,-2.5)\,;(-2.5,2.5)\,;(2.5,10)$

In an ideal case, the mixed event distribution is expected to have a constant flat distribution as function of $\Delta\phi$ and a triangular shaped distribution in $\Delta\eta$ deriving from the limited η acceptance of the detector. In case, instead of detector inefficient regions, or holes, in the same angular position for D meson and associated tracks, these structures produce an excess of correlations at $\Delta\phi = 0$ in the $\Delta\phi$ distribution. The obtained distribution is used as a weight in each correlation bin, i.e, the corrected correlation distribution is calculated as follows:

$$\frac{dN^{corr}(\Delta\phi\Delta\eta)}{d\Delta\phi d\Delta\eta} = \frac{\frac{dN^{SE}(\Delta\phi\Delta\eta)}{d\Delta\phi d\Delta\eta}}{\frac{dN^{ME}(\Delta\phi\Delta\eta)}{d\Delta\phi d\Delta\eta}} \frac{dN^{ME}(0,0)}{d\Delta\phi d\Delta\eta} \tag{4}$$

In the previous equation, the last term stands for the average of the bins in the region $-0.2 < \Delta\eta < 0.2$, $-0.2 < \Delta\phi < 0.2$ (multiple bins are used to minimize the effect of statistical fluctuations on the normalization of the mixed-event plots). This kind of normalization, adopted in the analysis of hadron-hadron correlations, relies on the fact that at $(\Delta\eta,\Delta\phi) = (0,0)$ the trigger and associated particle experience the same detector effects. In the D meson case this is true only on average and not at very low p_{T}, since D mesons are recontructed from particles that can go in different detector region. However, $(\Delta\eta,\Delta\phi) = (0,0)$ is in any case the region with maximum efficiency for the pairs (both correlated and uncorrelated). Thus the same convention was adopted.

The mixed-event correlation distributions are built in both D meson signal and sideband regions. Both are corrected with the relative distributions. An example of the mixed event distribution is shown in Fig. 1 (middle panels). The expected triangular shape in $\Delta\eta$ addresses the effect of the limited detector pseudo-rapidity acceptance. Note that the mixed-event distribution is limited to the interval $|\Delta\eta| < 1$: the decision to limit the mixed-event correction, and thus the whole analysis, to this range was taken in order to avoid the so-called "wing effect", i.e. the wing-like structures arising in the correlation distribution at large $\Delta\eta$ due to the limited filling of the correlation bins in that region.

Figure 1: $(\Delta\phi,\Delta\eta)$ correlation in the Sidebands and Signal region from Single Event and Mixing Event analysis for low p_T: $3 < p_T^{\mathrm{D}^+} < 5GeV/c$ with associated track p_T threshold 0.3 GeV/c

Figure 2: $(\Delta\phi,\Delta\eta)$ correlation in the Sidebands and Signal region from Single Event and Mixing Event analysis for mid p_T: $5 < p_T^{\mathrm{D}^+} < 8GeV/c$ with associcated track p_T threshold 0.3 GeV/c

Figure 3: $(\Delta\phi,\Delta\eta)$ correlation in the Sidebands and Signal region from Single Event and Mixing Event analysis for high p_T: $8 < p_T^{\mathrm{D}^+} < 16GeV/c$ with associcated track p_T threshold 0.3 GeV/c

Figures 1, 2, 3 show the 2D correlation in Sideband Region and Signal region from SE and ME analysis for D^+ meson in different p_T region.

3.2.2 Tracking and D-meson trigger efficiency

(i) Tracking efficiency: is calculated by obtaining the ratio between the yield at the reconstructed level and generated level, for a defined "type" of particles (in our case non-identified particles) and it is estimated differentially in p_T, η, and z_{vtx} of the event.
Implementation : tracking efficiency maps are produced as TH3D histograms (p_T, η, z_{vtx}) obtained from MC analysis on the minimum-bias samples LHC17a2b_fast and LHC17a2b_cent_woSDD, and applying at reconstructed level the track selections (summarized in Table. 2). These efficiency maps are used in the analysis tasks to extract single track efficiencies; each correlation pairs found in the data analysis is inserted in correlation plots with a weight of **1/efficiency value**. Example plots of the tracking efficiencies as a function of p_T are shown in Fig. **??**.

Figure 4: p_T efficiency for standard track selection.

Details of cuts at event level and particle selection at different steps are listed in Table. 2 .

MC Generated	
Stages	Cuts
1.MC Part with Generated Cuts	**After Event Selection** Charge PDG Code Physical Primary
2. MC Part with Kine Cuts	**Kinematics Cuts** -0.8$<\eta<$0.8 pT $>$ 0.3 (GeV/c)
MC Reconstructed	
4. Reco tracks	**After Event Selection** Physical Primary
5. Reco tracks with Kine Cuts	**Kinematics Cuts** -0.8$<\eta<$0.8 pT $>$ 0.3 (GeV/c)
6. MC true with Quality Cuts	**Quality Cuts** SetRequireSigmaToVertex(kFALSE) SetDCAToVertex2D(kFALSE) SetMinNCrossedRowsTPC(70) SetMinRatioCrossedRowsOverFindableClustersTPC(0.8) SetMinNClustersITS(3) SetMaxChi2PerClusterTPC(4) SetMaxDCAToVertexZ(1) SetMaxDCAToVertexXY(0.25) SetRequireTPCRefit(TRUE) SetRequireITSRefit(FALSE)
7. Reco tracks with Quality Cuts	**Same as step 6**

Table 2: Single Track Efficiency cuts detail

(ii) D Meson efficiency - Due to limited statistics, the correlation analysis is performed in quite wide p_T bins and in each of them the reconstruction and selection efficiency of D mesons is not flat (Fig. 6, 5), in particular in the lower p_T region. We correct for the p_T dependence of the trigger efficiency within each p_T-bin. This correction is applied online, by using a map of D meson efficiency as a function of p_T and event multiplicity (in terms of SPD tracklets in $|\eta| < 1$) extracted from the enriched Monte Carlo sample LHC17d2a_fast_new. While running the analysis, each correlation entry is weighted by **1/trigger efficiency**. It was observed that multiplicity dependence of the efficiency does not bias the extraction of the signal yield from the invariant mass distributions (which, as anticipated, are also weighted in the same manner). Efficiency plots for D^0, D^+ and D^{*+} mesons are shown in Fig. **??**, Fig. 6 and 7.

Figure 5: Top panel: (p_T, multiplicity) dependence (left) and p_T dependence (right) of prompt D^0 meson efficiency. Bottom panels: multiplicity dependence of D^0 meson efficiency for three D^0 p_T ranges: 3-4 GeV/c (left), 5-6 GeV/c (center), 8-12 GeV/c (right). For tracklet multiplicity$>$ 120, due to the limited statistics, the efficiency value is fixed to the one obtained for 90$<$tracklet multiplicity$<$120.

Figure 6: Top panel: (p_T, multiplicity) dependence of D^+ meson efficiency. Bottom panels: D^+ meson efficiency in multiplicity for three D^+ $p_T$ranges: 3-5 GeV/c (left), 5-8 GeV/c (center), 8-16 GeV/c (right).

Figure 7: Top panel: (p_T, multiplicity) dependence (left) and p_T dependence (right) of prompt D^{*+} meson efficiency. Bottom panels: multiplicity dependence of D^{*+} meson efficiency for three D^{*+} p_T ranges: 3-4 GeV/c (left), 5-6 GeV/c (center), 8-12 GeV/c (right). For tracklet multiplicity$>$ 120, due to the limited statistics, the efficiency value is fixed to the one obtained for 90$<$tracklet multiplicity$<$120.

3.2.3 Beauty feed-down

The contribution of correlations of D meson from b-hadron decay is subtracted from the data correlation distributions as:

$$\tilde{C}_{\text{prompt D}}(\Delta\phi) = \frac{1}{f_{\text{prompt}}}\left(\tilde{C}_{\text{inclusive}}(\Delta\phi) - (1 - f_{\text{prompt}})\tilde{C}^{\text{MC templ}}_{\text{feed-down}}(\Delta\phi)\right). \quad (5)$$

In the above equation, $\tilde{C}_{\text{inclusive}}(\Delta\phi)$ and $\tilde{C}_{\text{prompt D}}(\Delta\phi)$ are per-trigger azimuthal correlation distributions before and after feed-down contribution subtraction, f_{prompt} is the fraction of prompt D meson and $\tilde{C}^{\text{MC templ}}_{\text{feed-down}}$ is a template of the azimuthal correlation distribution for the feed-down component obtained from home-made Monte Carlo simulation at generated level, using PYTHIA6 with Perugia2011 tune. In order to avoid biases related to the different event multiplicity in real and simulated events, the correlation distribution was shifted to have its minimum coinciding with the baseline of the data azimuthal-correlation distribution before feed-down subtraction. The value of f_{prompt}, which depends on D-meson species and varies as a function of the p_T, is estimated on the basis of FONLL predictions for the production of feed-down D mesons at central rapidity, in pp collisions at $\sqrt{(}s) = 5$ TeV, and using the reconstruction efficiency of prompt and feed-down D mesons, following the so-called N_b approach defined in [6]. Typical values ranges are about 8-10% for the D^0, about 5% for the D^+ and **XXXX** percent for the D^{*+}. The procedure adopted is the same as what done in pp: however, in p–Pb, in order to consider a possible non-zero v_2-like modulation of the baseline, a range of $0 < v_2 < 0.2$ values for tracks and for secondary D mesons is considered for the systematic uncerainty evaluation (using an hypothesis of 0 for both cases for central values).

SOME TEMPLATE PLOTS HAVE TO BE ADDED HERE

4 Systematic uncertainties and checks of analysis consistency

5 Results

5.1 Comparing the three D meson correlation distributions

To check the compatibility of the three D meson analyses, Figure 8 shows the corrected azimuthal correlation distributions respectively for D^0-h, D^{*+}-h and D^+-h (except for the feed-down subtraction, on the data sample used in the analysis. Results are shown for $3 < D\ p_{\rm T} < 5$ GeV/c, $5 < D\ p_{\rm T} < 8$ GeV/c, $8 < D\ p_{\rm T} < 16$ GeV/c and $16 < D\ p_{\rm T} < 24$ GeV/c with associated tracks $p_{\rm T} > 0.3$, $p_{\rm T} > 1$, $0.3 < p_{\rm T} < 1$ GeV/c, $1 < p_{\rm T} < 2$ GeV/c, $2 < p_{\rm T} < 3$ GeV/c and $p_{\rm T} > 3$ GeV/c.

Figure 8: Superimposition of the corrected distribution of D-hadrons azimuthal correlations for the three species (apart from feed-down and purity), from analysis on the data sample, for the analyzed D-meson and associated track $p_{\rm T}$ ranges (Column-Left: $5 < {\rm D}^0\ p_{\rm T} < 8$ GeV/c, Column-Right: $8 < {\rm D}^0\ p_{\rm T} < 16$ GeV/c) and associated tracks $p_{\rm T}$ ranges (Row1: $>$0.3 GeV/c, Row2: 0.3 to 1 GeV/c, Row3: $>$1.0 GeV/c)

.

An agreement of the distributions from the three mesons within the uncertainties is found in all the kinematic ranges.

Despite being evaluated in the full 2π range, the range of final results was then reduced to $[0,\pi]$ radians, reflecting the points outside that range over the value of 0. This allowed to reduce the impact of statistical fluctuations on the data points (supposing equal statistics for a pair of symmetric bins, after the reflection the relative statistical uncertainty for the resulting bin is reduced by a factor $1/\sqrt{2}$).

5.2 Average of $\rm D^0$, $\rm D^+$ and $\rm D^{*+}$ results

Given the compatibility within the uncertainties among the $\rm D^0$, $\rm D^+$ and $\rm D^{*+}$ azimuthal correlations, and since no large differences are visible in the correlation distributions observed in Monte Carlo simulations based on Pythia with Perugia0, 2010 and 2011 tunes[2], it was possible to perform a weighted average (eq. 6) of the azimuthal correlation distributions of $\rm D^0$, $\rm D^+$ and $\rm D^{*+}$, in order to reduce the overall uncertainties. Although some correlation between the mesons could be present (about the 30% of the $\rm D^0$, and also part of the $\rm D^+$, come from $\rm D^{*+}$ decays), the three selected D-meson samples can be treated as uncorrelated. The inverse of the sum in quadrature of the statistical uncertainty and of the S and B extraction uncertainties was used as weight.

$$\left\langle \frac{1}{N_{\rm D}} \frac{dN^{\rm assoc}}{dp_{\rm T}} \right\rangle_{Dmesons} = \frac{\sum_{\rm i=meson} w_i \frac{1}{N_{\rm D}} \frac{dN_i^{\rm assoc}}{d\Delta\phi}}{\sum_{\rm i=meson} w_i} \quad , w_i = \frac{1}{\sigma^2_{i,\rm stat} + \sigma^2_{i,\rm uncorr.syst.}} \tag{6}$$

The statistical uncertainty and the uncertainty on the S and B extraction on the average were then recalculated using the following formula

$$\sigma^2 = \frac{1}{n_{\rm D}} \frac{\sum_{\rm i=meson} w_i \sigma_i^2}{\sum_{\rm i=meson} w_i} \tag{7}$$

where $n_{\rm D}$ is the number of mesons considered in the average. It can be observed that for $\sigma_i^2 = 1/w_i$ the formula coincides with the standard one giving the uncertainty on a weighted average. The contribution to the average systematic uncertainty for those uncertainty sources not included in the weight definition, was evaluated via error propagation on the formula of the weighted average (6), resulting in equation (8) and (9) for sources considered uncorrelated and correlated among the mesons. In particular, the

[2] A slight near side hierarchy is present among the three meson results, with $\rm D^{*+}$ meson having a lower peak amplitude than $\rm D^0$ and $\rm D^+$. It was verified that this is induced by the presence of $\rm D^0$ and $\rm D^+$ mesons coming from $\rm D^{*+}$, the latter having on average a larger p_T and coming, hence, on average, from a larger p_T quark parton, which fragments in slightly more tracks in the near-side.

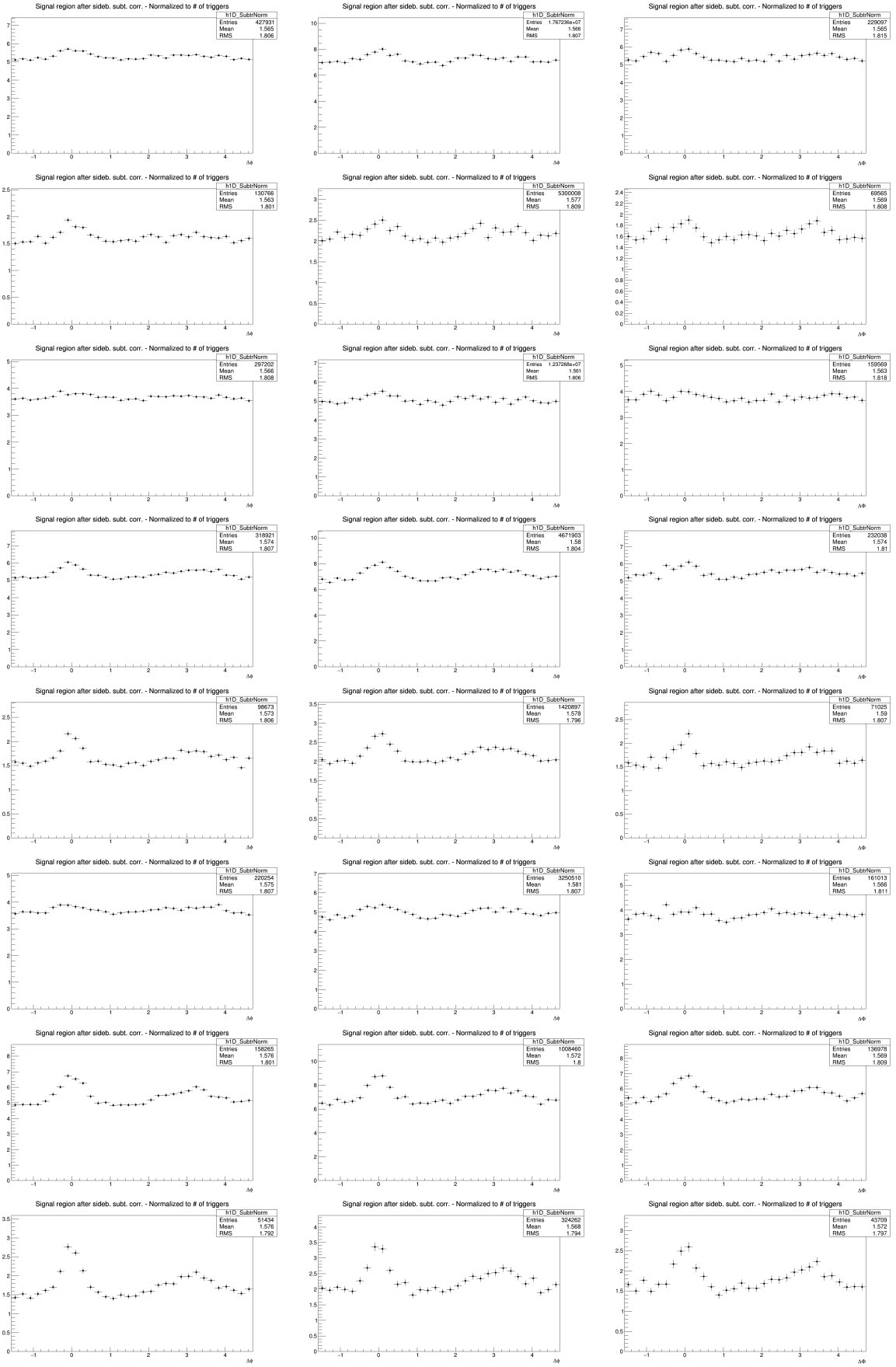
Signal region after sideb. subt. corr. - Normalized to # of triggers
h1D_SubtrNorm
Entries 427931
Mean 1.565
RMS 1.806
Signal region after sideb. subt. corr. - Normalized to # of triggers
h1D_SubtrNorm
Entries 1.767296e+07
Mean 1.566
RMS 1.807
Signal region after sideb. subt. corr. - Normalized to # of triggers
h1D_SubtrNorm
Entries 229097
Mean 1.565
RMS 1.815
Signal region after sideb. subt. corr. - Normalized to # of triggers
h1D_SubtrNorm
Entries 130766
Mean 1.563
RMS 1.801
Signal region after sideb. subt. corr. - Normalized to # of triggers
h1D_SubtrNorm
Entries 5300008
Mean 1.577
RMS 1.809
Signal region after sideb. subt. corr. - Normalized to # of triggers
h1D_SubtrNorm
Entries 69565
Mean 1.569
RMS 1.808
Signal region after sideb. subt. corr. - Normalized to # of triggers
h1D_SubtrNorm
Entries 297202
Mean 1.566
RMS 1.808
Signal region after sideb. subt. corr. - Normalized to # of triggers
h1D_SubtrNorm
Entries 1.237268e+07
Mean 1.561
RMS 1.806
Signal region after sideb. subt. corr. - Normalized to # of triggers
h1D_SubtrNorm
Entries 159569
Mean 1.563
RMS 1.818
Signal region after sideb. subt. corr. - Normalized to # of triggers
h1D_SubtrNorm
Entries 318921
Mean 1.574
RMS 1.807
Signal region after sideb. subt. corr. - Normalized to # of triggers
h1D_SubtrNorm
Entries 4671903
Mean 1.58
RMS 1.804
Signal region after sideb. subt. corr. - Normalized to # of triggers
h1D_SubtrNorm
Entries 232038
Mean 1.574
RMS 1.81
Signal region after sideb. subt. corr. - Normalized to # of triggers
h1D_SubtrNorm
Entries 98673
Mean 1.573
RMS 1.806
Signal region after sideb. subt. corr. - Normalized to # of triggers
h1D_SubtrNorm
Entries 1420897
Mean 1.578
RMS 1.796
Signal region after sideb. subt. corr. - Normalized to # of triggers
h1D_SubtrNorm
Entries 71025
Mean 1.59
RMS 1.807
Signal region after sideb. subt. corr. - Normalized to # of triggers
h1D_SubtrNorm
Entries 220254
Mean 1.575
RMS 1.807
Signal region after sideb. subt. corr. - Normalized to # of triggers
h1D_SubtrNorm
Entries 3250510
Mean 1.581
RMS 1.807
Signal region after sideb. subt. corr. - Normalized to # of triggers
h1D_SubtrNorm
Entries 161013
Mean 1.566
RMS 1.811
Signal region after sideb. subt. corr. - Normalized to # of triggers
h1D_SubtrNorm
Entries 158265
Mean 1.576
RMS 1.801
Signal region after sideb. subt. corr. - Normalized to # of triggers
h1D_SubtrNorm
Entries 1008460
Mean 1.572
RMS 1.8
Signal region after sideb. subt. corr. - Normalized to # of triggers
h1D_SubtrNorm
Entries 136978
Mean 1.569
RMS 1.809
Signal region after sideb. subt. corr. - Normalized to # of triggers
h1D_SubtrNorm
Entries 51434
Mean 1.576
RMS 1.792
Signal region after sideb. subt. corr. - Normalized to # of triggers
h1D_SubtrNorm
Entries 324262
Mean 1.568
RMS 1.794
Signal region after sideb. subt. corr. - Normalized to # of triggers
h1D_SubtrNorm
Entries 43709
Mean 1.572
RMS 1.797

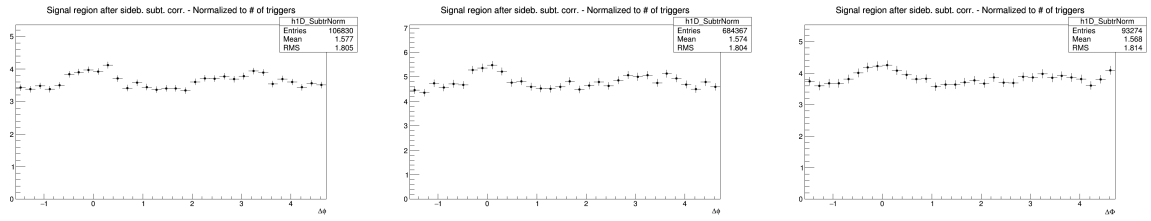

Figure 9: Comparison of D^0, D^+ and D^{*+}-hadron correlation, for the D meson p_T ranges $5 < D\ p_T < 8$ GeV/c and $8 < D\ p_T < 16$ GeV/c, with associated track transverse momentum in ranges $0.3 < p_T < 1$ GeV/c and $p_T > 1$ GeV/c.

uncertainties on the associated track reconstruction efficiency, on the contamination from secondary, on the feed-down subtraction, and that resulting from the Monte Carlo closure test were considered fully correlated among the mesons, while those deriving from the yield extraction (included in the weight definition) and on the D meson reconstruction and selection efficiency were treated as uncorrelated.

$$\sigma^2 = \frac{\sum_{\text{i=meson}} w_i^2 \sigma_i^2}{\left(\sum_{\text{i=meson}} w_i\right)^2} \tag{8}$$

$$\sigma = \frac{\sum_{\text{i=meson}} w_i \sigma_i}{\sum_{\text{i=meson}} w_i} \tag{9}$$

Figure 10 shows the averages of the azimuthal correlation distributions of D^0, D^+ and D^{*+} and charged particles with $p_T > 0.3$ GeV/c, $0.3 < p_T < 1$ GeV/c, $p_T > 1$ GeV/c, $1 < p_T < 2$ GeV/c, $2 < p_T < 3$ GeV/c, $p_T < 3$ GeV/c in the D meson p_T ranges $3 < p_T < 5$ GeV/c, $5 < p_T < 8$ GeV/c, $8 < p_T < 16$ GeV/c and $16 < p_T < 24$ GeV/c. As expected, a rising trend of the height of the near-side peak with increasing D-meson p_T is observed, together with a decrease of the baseline level with increasing p_T of the associated tracks.

Figure 10: Average of D^0, D^+ and D^{*+} azimuthal correlation distributions, in the D meson p_T ranges $5 < p_T < 8$ GeV/c and $8 < p_T < 16$ GeV/c, with associated tracks with $p_T > 0.3$ GeV/c, $p_T > 1$ GeV/c and $0.3 < p_T < 1$ GeV/c.

The usage of weighted average requires, as an underlying assumption, identical results expected for different species (or, at least, compatible within the uncertainties). **In case this assumption is not verified, an arithmetic average has to be computed instead, which does not rely on any assumption. As a drawback, the arithmetic average shows higher statistical uncertainties. Anyway, the distributions obtained evaluating the averages with the two approaches were found to be compatible, as shown in Figure ?? for two kinematic cases. TO BE DECIDED WHETHER TO KEEP THIS (DEPENDS IF I HAVE TIME TO DO THE FIGURES).**

5.3 Nearside associated yield, nearside width and baseline as function of the D meson p_T

In order to extract quantitative and physical information from the data correlation patterns, the averaged D-h correlation distributions are fitted with two Gaussian functions (with means fixed at $\Delta\phi$=0 and $\Delta\phi$=π values), plus a constant term (baseline). A periodicity condition is also applied to the fit function to obtain the same value at the bounds of 2π range. The expression of the fit expression is reported below (equation 10):

$$f(\Delta\phi) = c + \frac{Y_{NS}}{\sqrt{2\pi}\sigma_{NS}} e^{\frac{(\Delta\phi-\mu_{NS})^2}{2\sigma_{NS}^2}} + \frac{Y_{AS}}{\sqrt{2\pi}\sigma_{AS}} e^{\frac{(\Delta\phi-\mu_{AS})^2}{2\sigma_{AS}^2}} \tag{10}$$

where baseline is calculated as the weighted average of the points lying in the so-called "transverse region", i.e. the interval $\frac{\pi}{4} < |\Delta\phi| < \frac{\pi}{2}$.

An example of the results from the fit is shown in Figure 5.3.

From the fit outcome is it possible to retrieve the near-side and away-side yield and widths (integral and sigma of the Gaussian functions, respectively), as well as the baseline height. The near-side observables give information on the multiplicity and angular spread of the tracks from the fragmentation of the charm jet which gave birth to the D-meson trigger, while at first order the away-side observables are related to the hadronization of the charm parton produced in the opposite direction (though the presence of NLO processes for charm production breaks the full validity of this assumption). The baseline value is a rough indicator of the underlying event multiplicity, though below the baseline level also charm and beauty-related pairs are contained (especially in cases of NLO production for the heavy quarks).

The evaluation of the systematic uncertainties on the observables obtained from the fits is performed as follows:

- The fits are repeated by changing the range of the trasverse region in which the baseline is evaluated. Alternate definitions of $\frac{\pi}{4} < |\Delta\phi| < \frac{3\pi}{8}$, $\frac{3\pi}{8} < |\Delta\phi| < \frac{\pi}{2}$ and $\frac{\pi}{4} < |\Delta\phi| < \frac{5\pi}{8}$ are considered.
- In addition, $\Delta\phi$ correlation points are shifted to the upped and lower bounds of their uncorrelated systematic boxes, and the refitted.
- The maximum variation of the parameters between the fit outcomes defined in the previous points is considered as systematic uncertainty for the near-side and away-side widths.
- For the estimation of the baseline and of the near-side and away-side yields, the previous value is added in quadrature with the $\Delta\phi$-correlated systematics in the correlation distributions, since these values are affected by a change in the global normalization of the distributions.

$$\sigma^{syst} = \sqrt{\left(Max\left(\Delta par^{ped.mode}, \Delta par^{\Delta\phi point}\right)\right)^2 + \left(\sigma^{corr}_{Syst}\right)^2} \tag{11}$$

5.3.1 Results for near-side yield, near-side width and baseline

Figures 11, 12, 14, 14 and 15 show the near-side associated yield, width (the sigma of the Gaussian part of the fit functions) and the height of the baseline, for the average correlation distributions, in the kinematic ranges studied in the analysis. For each kinematic range, the correspondent plot showing the systematic uncertainty of the considered observable from the variation of the fit procedure is reported as well (which is the full systematic uncertainty for the widths). Figures **??**, **??**,and 18 show the full systematic uncertainties for yields and baseline, with the breakdown of fit variation and $\Delta\phi$ correlated systematic uncertainties.

Figure 11: Near side yield p_{T}(D) trend for the D-meson average, extracted from fit to the azimuthal correlation distributions, for all the analyzed kinematic ranges of associated track p_{T}. In the right column, for each kinematic region the systematic uncertainties coming from the variation of the fit procedure are shown.

Figure 12: Near side width p_{T}(D) trend for the D-meson average, extracted from fit to the azimuthal correlation distributions, for all the analyzed kinematic ranges of associated track p_{T}. In the right column, for each kinematic region the systematic uncertainties coming from the variation of the fit procedure are shown.

Figure 13: Away side yield p_{T}(D) trend for the D-meson average, extracted from fit to the azimuthal correlation distributions, for all the analyzed kinematic ranges of associated track p_{T}. In the right column, for each kinematic region the systematic uncertainties coming from the variation of the fit procedure are shown.

Figure 14: Away side width p_{T}(D) trend for the D-meson average, extracted from fit to the azimuthal correlation distributions, for all the analyzed kinematic ranges of associated track p_{T}. In the right column, for each kinematic region the systematic uncertainties coming from the variation of the fit procedure are shown.

Figure 15: Baseline height trend for the D-meson average, extracted from fit to the azimuthal correlation distributions, for all the analyzed kinematic ranges of associated track p_{T}. In the right column, for each kinematic region the systematic uncertainties coming from the variation of the fit procedure are shown.

Figure 16: Total systematic uncertainty, and its component, for near-side yields in the different kinematic ranges analyzed

6 Conclusions

text

Figure 17: Total systematic uncertainty, and its component, for near-side widths in the different kinematic ranges analyzed

Figure 18: Total systematic uncertainty, and its component, for baseline heights in the different kinematic ranges analyzed.

7 Bibliography

References

[1] J. Adam et al. [ALICE Collaboration], Nature Physics (2017) doi:10.1038/nphys4111.

[2] [E791 Collaboration],Correlations between D and $\bar{D}$ mesons produced in 500GeV π -nucleon interactions; EPJdirect C1 (2008)

[3] [CDF Collaboration], Measurement of Charm Meson pair Cross Section; CDF-Note 8621 2006.

[4] X.Zhu, N.Xu, P.Zhuang, Phys.Rev.Lett.100:152301,2008, arXiv:0709.0157.

[5] M. Nahrgang, J. Aichelin, P. B. Gossiaux, K. Werner, arXiv:1305.3823.

[6] B. Abelev et al. [ALICE Collaboration], JHEP **01** (2012) 128.